# Rigid body molecular dynamics with nonholonomic constraints: Molecular thermostat algorithms

Ramzi Kutteh* and R. B. Jones
*Department of Physics, Queen Mary and Westfield College, University of London, Mile End Road, London E1 4NS, United Kingdom*
(Received 20 September 1999)

Generalized Euler equations and center of mass equations are derived to describe the motion of a rigid body under general nonholonomic constraints. These equations provide a basis for developing algorithms for rigid body molecular dynamics (MD) simulations with nonholonomic constraints. In particular, two distinct molecular thermostat algorithms for constant temperature rigid body MD simulations are described. Both algorithms ensure satisfaction of the temperature constraint at every MD time step, without introducing additional numerical errors into the center of mass velocities or angular velocities. Results from constant temperature MD simulations of a system of 500 methylene chloride ($CH_2Cl_2$) rigid molecules using both thermostats are presented, exhibiting their efficiency and accuracy. Finally, a generalized Gauss's principle of least constraint is derived, to establish a formal connection between the molecular approach described here for incorporating nonholonomic constraints in MD simulations and previous atomistic approaches.

PACS number(s): 02.70.Ns, 05.10.−a, 07.05.Tp, 02.70.−c

## I. INTRODUCTION

Nonholonomic constraints involving velocities are commonly used [1–3] in equilibrium and nonequilibrium molecular dynamics (MD) simulations. It is often desirable to impose holonomic and nonholonomic constraints simultaneously in a MD simulation. Either of two methods can be used for this purpose.

First, both the holonomic and nonholonomic constraints can be implemented explicitly [4,5] by means of Lagrange multiplier techniques, which are essentially generalizations to additional nonholonomic constraints of approaches [6–9] developed previously for explicit implementation of holonomic constraints only. For example, the popular SHAKE algorithm [6,7] for holonomic constraints is generalized to a GSHAKE algorithm [4,5] for handling both holonomic and nonholonomic constraints. This first method, so-called atomistic approach, is practical for totally or partially rigid molecular models, as well as for purely nonholonomic constraints, of course.

Second, for totally rigid molecular models, it is computationally advantageous in some situations [1,9,10] to implement the holonomic rigidity constraints implicitly, by means of any of a variety of available rigid body MD methods [1,10–14], while still incorporating the nonholonomic constraints explicitly with the Lagrange multiplier technique. We shall refer to this alternative approach of imposing nonholonomic constraints in rigid body MD simulations as the molecular approach. It is our objective here to first derive equations of motion for rigid molecules under explicitly treated general nonholonomic constraints, and then to develop, based on these equations, two distinct molecular thermostat algorithms for constant kinetic (i.e., instantaneous) temperature rigid body MD simulations. It is worth noting at the outset that although a number of sophisticated rigid body algorithms [10–14] and semirigid body algorithms [15,16] for MD simulations have been proposed, the molecular thermostat algorithms described here are based on the basic quaternion rigid body algorithm [1,3], in order to illustrate most clearly and simply the additions required to go from a pure rigid body algorithm to a molecular thermostat algorithm based on it. The extension of the basic ideas presented here to the more sophisticated rigid body algorithms is, in principle at least, feasible.

Classical mechanics treatments of nonholonomic constraints [17,18] typically involve rigid bodies with rolling (without slipping) constraints (e.g., rolling sphere or disk on a surface) and are consequently all linear in the velocities. We are interested here, however, in describing the dynamics of rigid molecular models subject to more general (nonlinear) nonholonomic constraints. Although actual mechanical examples of nonlinear nonholonomic constraints are rare [17], computer simulations provide in contrast a flexible tool for imposing whatever forms of nonholonomic constraints necessary to simulate desirable conditions. In particular, a common form of a nonholonomic constraint in equilibrium and nonequilibrium MD simulations is the constant kinetic temperature constraint, nonlinear in the velocities.

Accordingly, we derive in Sec. II generalized equations of motion of a rigid body subject to general nonholonomic constraints. Using these equations, we develop in Sec. III a predictor-corrector quaternion thermostat algorithm for rigid body MD with a nonholonomic constant temperature constraint. However, when this basic thermostat algorithm is applied in MD simulations, the constant temperature constraint diverges progressively from its constraint value, as illustrated numerically in Sec. V. This numerical drift in the constraint is expected [1,4,5,19] because of the truncation error inherent in any numerical integration algorithm used to solve the constrained equations of motion. Two distinct approaches are developed here to deal with the constraint drift. First, we describe a correction technique for use with the basic thermostat algorithm, which eliminates the numerical

*Author to whom correspondence should be addressed. Electronic address: r.kutteh@qmw.ac.uk

 

drift without introducing additional numerical errors in the process, as shown in Appendix A. Second, in Sec. IV, an alternative thermostat algorithm is described where the approximate, rather than actual, constraint forces and torques are computed to ensure satisfaction of the constant temperature constraint at every MD step, again without introducing additional numerical errors in the process, as shown in Appendix B. As will be seen, these two distinct molecular approaches are formally analogous to counterpart atomistic approaches for imposing holonomic and nonholonomic constraints in MD simulations. In particular, these two molecular approaches are analogous to the analytical method [6,9] (albeit with a drift correction scheme) and the method of undetermined parameters [6,7,9], respectively, for imposing purely holonomic constraints in MD simulations. They are also analogous to the direct approach [4,5] (again with a drift correction scheme) and the undetermined parameters approach [4,5], respectively, for imposing additional nonholonomic constraints. In Sec. V, we present numerical results from constant kinetic temperature MD simulations of a system of 500 Lennard-Jones rigid molecules ($CH_2Cl_2$), which exhibit the relative performance of all three molecular thermostat algorithms mentioned above. Finally, a generalized Gauss principle of least constraint is derived in Appendix C, to furnish a common framework for the aforementioned previous atomistic methods [4,5] and the present molecular approach for incorporating nonholonomic constraints in MD simulations.

## II. EQUATIONS OF MOTION

In the following derivation we make use of two distinct coordinate systems: a laboratory coordinate system with origin $O$ and a body-fixed principal axes system with origin $O'$ at the body center of mass. Consider a rigid body with mass $M$ and configuration specified by six generalized coordinates $q_i$, where $q_1=x, q_2=y, q_3=z$ are the Cartesian coordinates of its center of mass in the laboratory coordinate system, and $q_4=\theta, q_5=\phi, q_6=\psi$, are the Euler angles giving the orientation of its principal axes relative to the laboratory axes. The Euler angles are defined here according to the common $x$ convention [20]. Let the rigid body be subject to the $n$ nonholonomic constraints

$$\sigma_l(q,\dot{q},t)=0; \quad l=1,\ldots,n, \tag{1}$$

where the dependence on all arguments is generally nonlinear. The constrained dynamics of this rigid body can be described by Appell's equations of motion [21–23]

$$\frac{d}{dt}\left(\frac{\partial T}{\partial \dot{q}_i}\right)-\frac{\partial T}{\partial q_i}=Q_i-\sum_{l=1}^{n}\lambda_l\frac{\partial \sigma_l}{\partial \dot{q}_i}=Q_i+Q_i^c; \quad i=1,\ldots,6, \tag{2}$$

where the $Q_i$ and $Q_i^c$ are the generalized applied forces and generalized constraint forces, respectively, $T$ is the total kinetic energy, and the $\lambda$'s are Lagrange multipliers. Historically, the atomistic approach for applying nonholonomic constraints in MD simulations exploited [1,2] Gauss's principle of least constraint [17,18,24,25]. To establish a unifying link with the molecular approach presented here, we derive in Appendix C a generalized form of Gauss's principle, and show that it leads to the same equations of motion, Eq. (2). In principle, the $n$ equations of constraints, Eq. (1), and the six equations of motion, Eq. (2), can be used to solve for the $n$ Lagrange multipliers and the six generalized coordinates describing the constrained dynamics. In practice, we would like first to convert Eq. (2) to a form that could serve as the basis for a MD algorithm. To this end, we adopt an approach similar to that [26] used for transforming from the Lagrangian to the Newtonian formulation of unconstrained rigid body dynamics. The total kinetic energy $T$ of the rigid body can be written as

$$T=\frac{1}{2}M\dot{\mathbf{r}}^2+T^r(\theta,\phi,\psi), \tag{3}$$

where $T^r$ is the rotational kinetic energy about the center of mass. Inserting Eq. (3) into Eq. (2), yields two sets of equations of motion. First, the equations for the translational motion of the center of mass are

$$M\ddot{\mathbf{r}}=\mathbf{F}-\sum_{l=1}^{n}\lambda_l\tilde{\nabla}\sigma_l=\mathbf{F}+\mathbf{F}^c, \tag{4}$$

where $\mathbf{F}$ and $\mathbf{F}^c$ are the applied force and constraint force on the rigid body, respectively, and $\tilde{\nabla}\equiv(\hat{\mathbf{x}}\partial/\partial\dot{x}+\hat{\mathbf{y}}\partial/\partial\dot{y}+\hat{\mathbf{z}}\partial/\partial\dot{z})$. Note that in the absence of the nonholonomic constraints in Eq. (1), Eq. (4) reduces to the familiar equation for the center of mass translation of an unconstrained rigid body. Second, the equations for the rotational motion about the center of mass are

$$\frac{d}{dt}\left(\frac{\partial T^r}{\partial \dot{q}_i}\right)-\frac{\partial T^r}{\partial q_i}=Q_i-\sum_{l=1}^{n}\lambda_l\frac{\partial \sigma_l}{\partial \dot{q}_i}=Q_i+Q_i^c; \quad i=4,\ldots,6, \tag{5}$$

where the $Q_i$ and $Q_i^c$ are the applied torques and constraint torques, respectively, associated with the corresponding Euler angles $q_i$ ($i=4,\ldots,6$). The choice of center of mass as point of reference in the rigid body allowed us to derive two sets of equations of motion, Eqs. (4) and (5), generally coupled through their right-hand sides. Next, the principal axes property of the body-fixed coordinate system is exploited to recast Eq. (5) in a form suitable for numerical implementation. Isolating the $\psi$ equation (i.e., $i=6$) of the set in Eq. (5), gives

$$\frac{d}{dt}\left(\frac{\partial T^r}{\partial \dot{\psi}}\right)-\frac{\partial T^r}{\partial \psi}=Q_\psi-\sum_{l=1}^{n}\lambda_l\frac{\partial \sigma_l}{\partial \dot{\psi}}=Q_\psi+Q_\psi^c. \tag{6}$$

In the principal axes system, the components of the angular velocity can be expressed as [20]

$$\begin{aligned}\omega_1&=\dot{\phi}\sin\theta\sin\psi+\dot{\theta}\cos\psi,\\ \omega_2&=\dot{\phi}\sin\theta\cos\psi-\dot{\theta}\sin\psi,\\ \omega_3&=\dot{\phi}\cos\theta+\dot{\psi}\end{aligned} \tag{7}$$

and the rotational kinetic energy is given by

$$T^r=\frac{1}{2}\sum_{i=1}^{3} I_i\omega_i^2, \tag{8}$$

where $I_1$, $I_2$, and $I_3$ are the principal moments of inertia relative to the center of mass. From Eq. (7) it follows that $\partial\omega_1/\partial\psi=\omega_2$ and $\partial\omega_2/\partial\psi=-\omega_1$. Therefore, by means of Eqs. (7) and (8) we can write

$$\frac{\partial T^r}{\partial\psi}=\sum_{i=1}^{3}\frac{\partial T^r}{\partial\omega_i}\frac{\partial\omega_i}{\partial\psi}=(I_1-I_2)\omega_1\omega_2;$$

$$\frac{\partial T^r}{\partial\dot{\psi}}=\sum_{i=1}^{3}\frac{\partial T^r}{\partial\omega_i}\frac{\partial\omega_i}{\partial\dot{\psi}}=I_3\omega_3. \tag{9}$$

Using Eq. (7), the derivatives of the Euler angles can be expressed in terms of the angular velocities and trigonometric functions of the Euler angles. Thus Eq. (1) can be recast in the more common form

$$\sigma_l(\mathbf{r},\dot{\mathbf{r}},\theta,\phi,\psi,\omega_1,\omega_2,\omega_3,t)=0; \quad l=1,\ldots,n \tag{10}$$

an important example of which is the constant kinetic temperature or energy constraint discussed in Sec. III. Using Eqs. (7) and (10), we have

$$Q_\psi^c=-\sum_{l=1}^{n}\lambda_l\frac{\partial\sigma_l}{\partial\dot{\psi}}=-\sum_{l=1}^{n}\lambda_l\sum_{i=1}^{3}\frac{\partial\sigma_l}{\partial\omega_i}\frac{\partial\omega_i}{\partial\dot{\psi}}=-\sum_{l=1}^{n}\lambda_l\frac{\partial\sigma_l}{\partial\omega_3}. \tag{11}$$

However, the torque associated with the $\psi$ Euler angle, $Q_\psi$, is equal [20,26] to the principal axis torque $N_3$. Therefore, inserting $Q_\psi=N_3$ and $Q_\psi^c=N_3^c$, together with Eqs. (9) and (11), into Eq. (6), yields

$$I_3\dot{\omega}_3-(I_1-I_2)\omega_1\omega_2=N_3-\sum_{l=1}^{n}\lambda_l\frac{\partial\sigma_l}{\partial\omega_3}=N_3+N_3^c. \tag{12}$$

Because the labeling of a principal axis as the three-axis is arbitrary, Eq. (12) can be cyclically permuted to obtain the remaining two rotational equations of motion. Hence the equations of motion describing the rotation of the nonholonomically constrained rigid body, about its center of mass, are given by

$$I_1\dot{\omega}_1-(I_2-I_3)\omega_2\omega_3=N_1-\sum_{l=1}^{n}\lambda_l\frac{\partial\sigma_l}{\partial\omega_1}=N_1+N_1^c,$$

$$I_2\dot{\omega}_2-(I_3-I_1)\omega_1\omega_3=N_2-\sum_{l=1}^{n}\lambda_l\frac{\partial\sigma_l}{\partial\omega_2}=N_2+N_2^c,$$

$$I_3\dot{\omega}_3-(I_1-I_2)\omega_1\omega_2=N_3-\sum_{l=1}^{n}\lambda_l\frac{\partial\sigma_l}{\partial\omega_3}=N_3+N_3^c. \tag{13}$$

In the absence of the nonholonomic constraints in Eq. (1), Eq. (13) reduces to the well known Euler equations [20] for the rotation of an unconstrained rigid body about its center of mass. Equations (4) and (13) must form the basis of any algorithm for MD simulations of rigid molecules under nonholonomic constraints, in the molecular approach. In particular, in the next section, we consider a predictor-corrector quaternion algorithm and a constant temperature constraint.

## III. THERMOSTAT ALGORITHM I

A common and important example of a nonholonomic constraint, both in equilibrium and nonequilibrium MD simulations, is the constant kinetic temperature constraint [1–3]. As discussed in the Introduction, atomistic algorithms for implementing this constraint in MD simulations, with or without additional holonomic constraints (e.g., bond length constraints, bond-angle constraints), have been recently described [4,5]. We now describe the first of two molecular thermostat algorithms for implementing it within the molecular approach for a system of rigid molecules. The extension of this algorithm to more than a single nonholonomic constraint and to other desirable forms of nonholonomic constraints is straightforward.

The basic thermostat algorithm (BTA) described first is based on a modification of the well known quaternion algorithm [1] for rigid body MD simulations. In practice, this BTA will suffer from numerical drift in the constant kinetic temperature constraint, as shown in Sec. V, because of the truncation error inherent in the numerical integration of the equations of motion. Accordingly, we follow the BTA with a correction technique where the center of mass velocities are corrected to ensure that the constant temperature constraint is satisfied, within a desired tolerance, at every MD time step. The BTA with this correction technique are referred to collectively as thermostat algorithm I (TA1).

### A. Basic thermostat algorithm

Consider a system of $N$ interacting rigid molecules subject to the nonholonomic constant kinetic temperature constraint

$$\sigma(\dot{\mathbf{r}},\omega_1,\omega_2,\omega_3)=\alpha\sum_{j=1}^{N}\left[M_j\dot{\mathbf{r}}_j^2+\sum_{i=1}^{3}I_i^j(\omega_i^j)^2\right]-\beta=0, \tag{14}$$

where $\beta$ is a desired constant kinetic temperature, $\alpha=1/(6N-N_c)k_B$, with $N_c$ equal to the total number of constraints, which is four in the present case, to account for conservation of total linear momentum and Eq. (14). Clearly, Eq. (14) is a special case of Eq. (10).

In the BTA, the kinetic temperature is initially brought to a desired value, typically by scaling the velocities [1], and then the algorithm attempts to maintain it constant during the MD simulation. Hence the constant kinetic temperature constraint is implemented instead simply by means of a constant kinetic energy constraint

$$\sigma'(\dot{\mathbf{r}},\omega_1,\omega_2,\omega_3)=\sum_{j=1}^{N}\left[\frac{1}{2}M_j\dot{\mathbf{r}}_j^2+\frac{1}{2}\sum_{i=1}^{3}I_i^j(\omega_i^j)^2\right]-\beta'=0. \tag{15}$$

From Eq. (4), the center of mass equations of motion are

$$M_j\ddot{\mathbf{r}}_j=\mathbf{F}_j-\lambda M_j\dot{\mathbf{r}}_j=\mathbf{F}_j+\mathbf{F}_j^c; \quad j=1,\ldots,N \tag{16}$$

and from Eq. (13), the equations for the rotation about the centers of mass are

$$
\begin{aligned}
&I_1^j\dot{\omega}_1^j-(I_2^j-I_3^j)\omega_2^j\omega_3^j=N_1^j-\lambda I_1^j\omega_1^j=N_1^j+(N_1^j)^c,\\
&I_2^j\dot{\omega}_2^j-(I_3^j-I_1^j)\omega_1^j\omega_3^j=N_2^j-\lambda I_2^j\omega_2^j=N_2^j+(N_2^j)^c,\\
&I_3^j\dot{\omega}_3^j-(I_1^j-I_2^j)\omega_1^j\omega_2^j=N_3^j-\lambda I_3^j\omega_3^j\\
&\qquad=N_3^j+(N_3^j)^c;\quad j=1,\ldots,N.
\end{aligned}
\tag{17}
$$

The numerical solution of these equations of motion is performed in two steps. First, the nonholonomic constraint forces, $\mathbf{F}^c$, and constraint torques $N_1^c$, $N_2^c$, and $N_3^c$, are evaluated. Second, the equations of motion are integrated numerically using the potential energy forces and torques together with the constraint forces and torques. The computation of the constraint forces and torques requires computation of the Lagrange multiplier $\lambda$. To this end, differentiating Eq. (15) with respect to time and inserting into the resulting equation the expression for $\ddot{\mathbf{r}}_j$ from Eq. (16) and the expressions for $\dot{\omega}_1^j$, $\dot{\omega}_2^j$, $\dot{\omega}_3^j$ from Eq. (17), gives

$$
\begin{aligned}
&\sum_{j=1}^{N}[\mathbf{F}_j-\lambda M_j\dot{\mathbf{r}}_j]\cdot\dot{\mathbf{r}}_j+\omega_1^j[N_1^j-\lambda I_1^j\omega_1^j+(I_2^j-I_3^j)\omega_2^j\omega_3^j]\\
&\quad+\omega_2^j[N_2^j-\lambda I_2^j\omega_2^j+(I_3^j-I_1^j)\omega_1^j\omega_3^j]\\
&\quad+\omega_3^j[N_3^j-\lambda I_3^j\omega_3^j+(I_1^j-I_2^j)\omega_1^j\omega_2^j]\\
&\quad=0.
\end{aligned}
\tag{18}
$$

Solving Eq. (18) for $\lambda$ yields

$$
\lambda=\frac{\sum_{j=1}^{N}\left[\mathbf{F}_j\cdot\dot{\mathbf{r}}_j+\sum_{i=1}^{3}\omega_i^jN_i^j\right]}{\sum_{j=1}^{N}\left[M_j\dot{\mathbf{r}}_j^2+\sum_{i=1}^{3}I_i^j(\omega_i^j)^2\right]}
\tag{19}
$$

By means of Eq. (19), the constraint forces, $\mathbf{F}^c$, and constraint torques, $N_1^c$, $N_2^c$ and $N_3^c$, can now be computed.

For the numerical integration of the constrained equations of motion, we adopt the predictor-corrector quaternion algorithm [1,10,11,13] commonly used in (unconstrained) rigid body MD simulations. The molecular orientation is given in terms of four quaternion parameters $q_i$ $(i=0,\ldots,3)$ subject to the normalization condition $q_0^2+q_1^2+q_2^2+q_3^2=1$. To integrate the equations of motion, the center of mass positions, the quaternions, and the angular velocities (and all their appropriate time derivatives) are first predicted using the stored values of these quantities and their required time derivatives. The quaternions are then typically renormalized to preserve orthogonality of the rotation matrix for the corresponding molecule

$$
\mathbf{A}=\begin{pmatrix}
q_0^2+q_1^2-q_2^2-q_3^2 & 2(q_1q_2+q_0q_3) & 2(q_1q_3-q_0q_2)\\
2(q_1q_2-q_0q_3) & q_0^2-q_1^2+q_2^2-q_3^2 & 2(q_2q_3+q_0q_1)\\
2(q_1q_3+q_0q_2) & 2(q_2q_3-q_0q_1) & q_0^2-q_1^2-q_2^2+q_3^2
\end{pmatrix}.
\tag{20}
$$

Multiplication of the principal axes components of the atomic positions with respect to the centers of mass, by $\mathbf{A}^{-1}(=\mathbf{A}^T)$ yields the laboratory frame components of the predicted atomic positions with respect to the centers of mass. These are then added to the corresponding predicted center of mass positions to give the predicted atomic positions in the laboratory frame. Subsequently, the force on each atom is computed and the total force $\mathbf{F}$ and total torque on each molecule are evaluated in the laboratory frame. The laboratory frame components of the total torque on each molecule are then multiplied by $\mathbf{A}$ to yield the necessary corresponding principal axes torques $N_1$, $N_2$, and $N_3$. Up to this point, the quaternion scheme described is simply the standard one. In Sec. IV, we will refer to this stage of the BTA as stage A. Now, however, the undetermined multiplier $\lambda$ is evaluated according to Eq. (19), and the constraint forces $\mathbf{F}^c$ and constraint torques $N_1^c$, $N_2^c$, and $N_3^c$ are computed. The constraint forces $\mathbf{F}^c$ and potential energy forces $\mathbf{F}$ are used in the corrector stage of the algorithm, based on Eq. (16), and the constraint torques $N_1^c$, $N_2^c$, and $N_3^c$, and potential energy torques $N_1$, $N_2$, and $N_3$, are used in the corrector stage, according to Eq. (17). Finally, the quaternions are corrected for each molecule according to the kinematic equations

$$
\begin{pmatrix}\dot{q}_0\\ \dot{q}_1\\ \dot{q}_2\\ \dot{q}_3\end{pmatrix}=\frac{1}{2}\begin{pmatrix}q_0 & -q_1 & -q_2 & -q_3\\ q_1 & q_0 & -q_3 & q_2\\ q_2 & q_3 & q_0 & -q_1\\ q_3 & -q_2 & q_1 & q_0\end{pmatrix}\begin{pmatrix}0\\ \omega_1\\ \omega_2\\ \omega_3\end{pmatrix}.
\tag{21}
$$

Note that through their $\lambda$ coupling, the corrector stage of Eq. (16) depends now explicitly on rotational quantities, while the corrector stage of Eq. (17) depends explicitly on translational ones. In Sec. V, we use a common combination of a third order Gear predictor-corrector for integrating the center

of mass equations of motion and a fourth order Gear predictor-corrector for the quaternions and principal angular velocities.

### B. Drift correction technique

As mentioned before, when the above BTA is applied in MD simulations, the constant kinetic temperature constraint, Eq. (14), diverges progressively from its constraint value $\beta$. Therefore, we describe next a technique for use following the BTA, which eliminates the numerical drift in the constraint at every MD time step. A truncated Taylor expansion of the center of mass velocities from the BTA, can be written as

$$\begin{aligned}\dot{\mathbf{r}}_i(t_0+\delta t) &= \dot{\mathbf{r}}_i(t_0)+\ddot{\mathbf{r}}_i(t_0)\,\delta t \\ &= \dot{\mathbf{r}}_i(t_0)+\frac{\delta t}{M_i}\mathbf{F}_i(t_0)-\delta t\lambda(t_0)\dot{\mathbf{r}}_i(t_0); \\ &\quad (i=1,\ldots,N),\end{aligned} \tag{22}$$

where use was made of Eq. (16). Introducing an additional term into Eq. (22), containing an unknown $\gamma$, gives

$$\begin{aligned}\dot{\mathbf{r}}_i(t_0+\delta t,\gamma) &= \dot{\mathbf{r}}_i(t_0)+\frac{\delta t}{M_i}\mathbf{F}_i(t_0)-\delta t\lambda(t_0)\dot{\mathbf{r}}_i(t_0)-\delta t\,\gamma\dot{\mathbf{r}}_i(t_0) \\ &= \dot{\mathbf{r}}_i(t_0+\delta t)-\delta t\,\gamma\dot{\mathbf{r}}_i(t_0); \quad (i=1,\ldots,N),\end{aligned} \tag{23}$$

where $\gamma$ is required to have a value such that the constraint, Eq. (14), is satisfied. Therefore Eq. (14) can be written as

$$\begin{aligned}&\sigma(\dot{\mathbf{r}}(t_0+\delta t,\gamma),\omega_1,\omega_2,\omega_3) \\ &\quad=\sigma(\dot{\mathbf{r}}(t_0+\delta t)-\delta t\,\gamma\dot{\mathbf{r}}(t_0),\omega_1,\omega_2,\omega_3)=0\end{aligned} \tag{24}$$

which is quadratic in the unknown $\gamma$, and where $\omega_1$, $\omega_2$, and $\omega_3$ are obtained from the BTA, of course. The solution $\gamma$ is substituted into Eq. (23) to provide the final constrained center of mass velocities. It is most convenient computationally to solve Eq. (24) iteratively for $\gamma$, essentially by Newton's method. To this end, consider a certain iteration, drop the $\gamma$ notation from $\dot{\mathbf{r}}_i(t_0+\delta t,\gamma)$ in Eq. (23), and let $\dot{\mathbf{r}}^{\rm old}(t_0+\delta t)$ include all changes made up to this point in the iteration. From Eq. (23), the new center of mass velocities obtained in the current iteration can be written as

$$\dot{\mathbf{r}}_i^{\rm new}(t_0+\delta t)=\dot{\mathbf{r}}_i^{\rm old}(t_0+\delta t)-\delta t\,\gamma^{\rm new}\dot{\mathbf{r}}_i(t_0); \quad (i=1,\ldots,N), \tag{25}$$

where the starting value of $\dot{\mathbf{r}}_i^{\rm old}(t_0+\delta t)$ is $\dot{\mathbf{r}}_i(t_0+\delta t)$ in Eq. (23), the center of mass velocities from the BTA, of course. Taylor expanding $\sigma(\dot{\mathbf{r}}^{\rm new}(t_0+\delta t),\omega_1,\omega_2,\omega_3)$ about $\dot{\mathbf{r}}^{\rm old}(t_0+\delta t)$ gives

$$\begin{aligned}&\sigma(\dot{\mathbf{r}}^{\rm old}(t_0+\delta t)-\delta t\,\gamma^{\rm new}\dot{\mathbf{r}}(t_0),\omega_1,\omega_2,\omega_3) \\ &\quad=\sigma(\dot{\mathbf{r}}^{\rm old}(t_0+\delta t),\omega_1,\omega_2,\omega_3) \\ &\qquad-\delta t\,\gamma^{\rm new}2\alpha\sum_{i=1}^{N}M_i\dot{\mathbf{r}}_i^{\rm old}(t_0+\delta t)\cdot\dot{\mathbf{r}}_i(t_0)+\cdots=0\end{aligned} \tag{26}$$

where the quadratic term is not shown explicitly. Neglecting the nonlinear term and solving for $\gamma^{\rm new}$ yields

$$\gamma^{\rm new}=[\delta t]^{-1}\frac{\sigma(\dot{\mathbf{r}}^{\rm old}(t_0+\delta t),\omega_1,\omega_2,\omega_3)}{2\alpha\sum_{i=1}^{N}M_i\dot{\mathbf{r}}_i^{\rm old}(t_0+\delta t)\cdot\dot{\mathbf{r}}_i(t_0)}. \tag{27}$$

Inserting Eq. (27) into Eq. (25) gives

$$\dot{\mathbf{r}}_i^{\rm new}(t_0+\delta t)=\dot{\mathbf{r}}_i^{\rm old}(t_0+\delta t)-\left(\frac{\alpha\sum_{j=1}^{N}\left\{M_j[\dot{\mathbf{r}}_j^{\rm old}(t_0+\delta t)]^2+\sum_{i=1}^{3}I_i^j(\omega_i^j)^2\right\}-\beta}{2\alpha\sum_{i=1}^{N}M_i\dot{\mathbf{r}}_i^{\rm old}(t_0+\delta t)\cdot\dot{\mathbf{r}}_i(t_0)}\right)\dot{\mathbf{r}}_i(t_0) \quad (i=1,\ldots,N). \tag{28}$$

Immediately following the BTA, the center of mass velocities are iterated according to Eq. (28) until the numerator in parentheses, representing the current value of the constraint function, is below a desired tolerance $\tau$. It is shown in Appendix A that, owing to the special form of the additional correction term introduced in Eq. (23), this correction technique, and hence the TA1, does not introduce into the center of mass velocities, errors of an order in the time step lower than already present in the BTA. Note in addition that this correction does not affect the BTA values of the angular velocities and, hence, of the quaternions.

## IV. THERMOSTAT ALGORITHM II

In the TA1 described in the previous section, the actual constraint forces, $\mathbf{F}^c$, and actual constraint torques, $N_1^c$, $N_2^c$, and $N_3^c$, were computed *a priori* at stage A of the BTA and used in the integration of the equations of motion, Eqs. (16) and (17). The constraint forces on the centers of mass were subsequently corrected, or approximated, to eliminate the numerical drift in the temperature constraint and ensure its satisfaction at every MD time step, as described in Sec. III B. We now describe an alternative thermostat algorithm II (TA2) where the approximate, rather than actual, constraint

forces and constraint torques are computed *a posteriori* to ensure satisfaction of the temperature constraint at every MD step. It is shown in Appendix B that the TA2 does not introduce, into the center of mass velocities or angular velocities, errors of an order in the time step lower than already present in the BTA. A comparison of the advantages of TA1 versus those of TA2 is given in Sec. V.

A truncated Taylor expansion of the center of mass velocities from the BTA is given by

$$\begin{aligned}\dot{\mathbf{r}}_i(t_0+\delta t) &= \dot{\mathbf{r}}_i(t_0)+\ddot{\mathbf{r}}_i(t_0)\,\delta t \\ &= \dot{\mathbf{r}}_i(t_0)+\frac{\delta t}{M_i}\mathbf{F}_i(t_0)-\delta t\lambda(t_0)\dot{\mathbf{r}}_i(t_0) \\ &= \dot{\mathbf{r}}_i'(t_0+\delta t)+\delta\dot{\mathbf{r}}_i(t_0+\delta t) \quad (i=1,\ldots,N),\end{aligned} \tag{29}$$

where the unconstrained center of mass velocity $\dot{\mathbf{r}}_i'(t_0+\delta t)$ denotes the sum of the first two terms. Similarly, a truncated Taylor expansion of the angular velocities from the BTA is given by

$$\begin{aligned}\omega_1^j(t_0+\delta t) &= \omega_1^j(t_0)+\dot{\omega}_1^j(t_0)\,\delta t \\ &= \omega_1^j(t_0)+\frac{\delta t}{I_1^j}[(I_2^j-I_3^j)\omega_2^j(t_0)\omega_3^j(t_0) \\ &\quad +N_1^j(t_0)]-\delta t\lambda(t_0)\omega_1^j(t_0) \\ &= \omega_1'^j(t_0+\delta t)+\delta\omega_1^j(t_0+\delta t) \quad (j=1,\ldots,N),\end{aligned} \tag{30}$$

where the unconstrained angular velocity $\omega_1'^j(t_0+\delta t)$ denotes the sum of the first two terms, and similar equations hold for $\omega_2^j$ and $\omega_3^j$. In the BTA, the constrained center of mass velocities, $\dot{\mathbf{r}}_i(t_0+\delta t)$, and constrained angular velocities, $\omega_i^j(t_0+\delta t)$, were evaluated by first computing $\lambda$ and then numerically integrating the equations of motion. Instead, we now compute the $\dot{\mathbf{r}}_i(t_0+\delta t)$ and $\omega_i^j(t_0+\delta t)$ from the two contributions in Eqs. (29) and (30), respectively.

First, the $\dot{\mathbf{r}}_i'(t_0+\delta t)$ and $\omega_i'^j(t_0+\delta t)$ are evaluated by numerically integrating the equations of motion using only the potential energy forces and torques at stage A of the BTA. Second, the $\delta\dot{\mathbf{r}}_i$ and $\delta\omega_i^j$ are chosen to ensure satisfaction of the constraint at every MD time step. To this end $\lambda(t_0)$ is replaced by an undetermined parameter, $\eta$, and Eqs. (29) and (30) become

$$\dot{\mathbf{r}}_i(t_0+\delta t)=\dot{\mathbf{r}}_i'(t_0+\delta t)-\delta t\,\eta\dot{\mathbf{r}}_i(t_0) \quad (i=1,\ldots,N) \tag{31}$$

and

$$\begin{aligned}\omega_i^j(t_0+\delta t) &= \omega_i'^j(t_0+\delta t)-\delta t\,\eta\omega_i^j(t_0) \\ &\quad (i=1,\ldots,3;\ j=1,\ldots,N),\end{aligned} \tag{32}$$

respectively, where $\eta$ is required to have a value such that Eq. (14) is satisfied. Hence Eq. (14) can be written as

$$\sigma(\dot{\mathbf{r}}'(t_0+\delta t)-\delta t\,\eta\dot{\mathbf{r}}(t_0),\omega_i'(t_0+\delta t)-\delta t\,\eta\omega_i(t_0))=0, \tag{33}$$

which is quadratic in the unknown $\eta$. The solution $\eta$ is substituted into Eqs. (31) and (32) to provide the constrained center of mass velocities and constrained angular velocities from the TA2. As in Sec. III B, it is most convenient computationally to solve Eq. (33) iteratively for $\eta$. Again, with $\dot{\mathbf{r}}^{\rm old}(t_0+\delta t)$ including all changes made up to this point in the iteration, the new center of mass velocities obtained in the current iteration can be written as

$$\dot{\mathbf{r}}_i^{\rm new}(t_0+\delta t)=\dot{\mathbf{r}}_i^{\rm old}(t_0+\delta t)-\delta t\,\eta^{\rm new}\dot{\mathbf{r}}_i(t_0) \quad (i=1,\ldots,N), \tag{34}$$

where the starting value of $\dot{\mathbf{r}}_i^{\rm old}(t_0+\delta t)$ is $\dot{\mathbf{r}}_i'(t_0+\delta t)$. Similarly, the new angular velocities obtained in the current iteration can be written as

$$\begin{aligned}\omega_i^{j,{\rm new}}(t_0+\delta t) &= \omega_i^{j,{\rm old}}(t_0+\delta t)-\delta t\,\eta^{\rm new}\omega_i^j(t_0) \\ &\quad (i=1,\ldots,3;\ \ j=1,\ldots,N),\end{aligned} \tag{35}$$

where the starting value of $\omega_i^{j,{\rm old}}(t_0+\delta t)$ is $\omega_i'^j(t_0+\delta t)$. Taylor expanding $\sigma(\dot{\mathbf{r}}^{\rm new}(t_0+\delta t),\omega_i^{\rm new}(t_0+\delta t))$ about $\dot{\mathbf{r}}^{\rm old}(t_0+\delta t)$ and $\omega_i^{\rm old}(t_0+\delta t)$ gives

$$\begin{aligned}&\sigma(\dot{\mathbf{r}}^{\rm old}(t_0+\delta t)-\delta t\,\eta^{\rm new}\dot{\mathbf{r}}(t_0),\omega_i^{\rm old}(t_0+\delta t)-\delta t\,\eta^{\rm new}\omega_i(t_0)) \\ &\quad=\sigma(\dot{\mathbf{r}}^{\rm old}(t_0+\delta t),\omega_i^{\rm old}(t_0+\delta t))-\delta t\,\eta^{\rm new}2\alpha \\ &\qquad\times\sum_{i=1}^{N}M_i\dot{\mathbf{r}}_i^{\rm old}(t_0+\delta t)\cdot\dot{\mathbf{r}}_i(t_0)-\delta t\,\eta^{\rm new}2\alpha \\ &\qquad\times\sum_{j=1}^{N}\sum_{i=1}^{3}I_i^j\omega_i^{j,{\rm old}}(t_0+\delta t)\omega_i^j(t_0)+\cdots=0,\end{aligned} \tag{36}$$

where the quadratic term is not shown explicitly. Neglecting the nonlinear term and solving for $\eta^{\rm new}$ yields

$$\eta^{\rm new}=[\delta t]^{-1}\frac{\sigma(\dot{\mathbf{r}}^{\rm old}(t_0+\delta t),\omega_i^{\rm old}(t_0+\delta t))}{2\alpha\sum_{j=1}^{N}\left[M_j\dot{\mathbf{r}}_j^{\rm old}(t_0+\delta t)\cdot\dot{\mathbf{r}}_j(t_0)+\sum_{i=1}^{3}I_i^j\omega_i^{j,{\rm old}}(t_0+\delta t)\omega_i^j(t_0)\right]}. \tag{37}$$

Inserting Eq. (37) into Eq. (34) gives

$$\dot{\mathbf{r}}_i^{\mathrm{new}}(t_0+\delta t)=\dot{\mathbf{r}}_i^{\mathrm{old}}(t_0+\delta t)-\left(\frac{\alpha\sum_{j=1}^{N}\left\{M_j[\dot{\mathbf{r}}_j^{\mathrm{old}}(t_0+\delta t)]^2+\sum_{i=1}^{3}I_i^j[\omega_i^{j,\mathrm{old}}(t_0+\delta t)]^2\right\}-\beta}{2\alpha\sum_{j=1}^{N}\left[M_j\dot{\mathbf{r}}_j^{\mathrm{old}}(t_0+\delta t)\cdot\dot{\mathbf{r}}_j(t_0)+\sum_{i=1}^{3}I_i^j\omega_i^{j,\mathrm{old}}(t_0+\delta t)\omega_i^j(t_0)\right]}\right)\dot{\mathbf{r}}_i(t_0)\quad(i=1,\ldots,N) \tag{38}$$

and into Eq. (35) gives

$$\omega_i^{j,\mathrm{new}}(t_0+\delta t)=\omega_i^{j,\mathrm{old}}(t_0+\delta t)-\left(\frac{\alpha\sum_{j=1}^{N}\left\{M_j[\dot{\mathbf{r}}_j^{\mathrm{old}}(t_0+\delta t)]^2+\sum_{i=1}^{3}I_i^j[\omega_i^{j,\mathrm{old}}(t_0+\delta t)]^2\right\}-\beta}{2\alpha\sum_{j=1}^{N}\left[M_j\dot{\mathbf{r}}_j^{\mathrm{old}}(t_0+\delta t)\cdot\dot{\mathbf{r}}_j(t_0)+\sum_{i=1}^{3}I_i^j\omega_i^{j,\mathrm{old}}(t_0+\delta t)\omega_i^j(t_0)\right]}\right)\omega_i^j(t_0)$$

$$(i=1,\ldots,3;\ \ j=1,\ldots,N). \tag{39}$$

The center of mass velocities and angular velocities are iterated according to Eqs. (38) and (39), respectively, until the numerator in parentheses, representing the current value of the constraint function, is below a desired tolerance $\tau$. It is shown in Appendix B that the center of mass velocity and angular velocity trajectories from the TA2 are numerically equivalent to the corresponding trajectories from the BTA, and hence, in light of the conclusion of Appendix A, are numerically equivalent to the corresponding trajectories from the TA1 also. After the constrained center of mass velocities and angular velocities are obtained as described above, the quaternions are corrected based on Eq. (21), as the final step in TA2.

## V. NUMERICAL RESULTS AND DISCUSSION

Numerical results are presented here to exhibit the properties of the molecular thermostat algorithms TA1 and TA2 and their relative performance. Constant energy MD simulations and constant kinetic temperature MD simulations were performed on a system of 500 rigid molecules interacting via a five-site Lennard-Jones 12-6 potential. Parameter values were chosen as those of methylene chloride, $CH_2Cl_2$, with geometry and potential parameters obtained from Ref. [27]. The five force sites are identical with the atomic positions in the molecule, and although a methylene chloride molecule is a nearly symmetric top molecule, strictly speaking its three principal moments of inertia, $I_1$, $I_2$, and $I_3$ are distinct. All simulations were performed with time step $\delta t=1$ fs. Periodic boundary conditions were imposed and a potential cutoff radius equal to half the box length was used. As commonly done [1], a third order Gear predictor-corrector was used for integrating the center of mass equations of motion, while a fourth order Gear predictor-corrector was adopted for the quaternions and principal angular velocities. The constant energy MD simulations were carried out at a density of 1.326 g/cm$^3$ and temperature of 293 K. The constant kinetic temperature simulations were performed at the same density, while the kinetic temperature was maintained fixed at 293 K using the TA1 or TA2.

First, to perform constant energy rigid body MD simulations at a state point specified typically by the density and temperature, it is common practice to maintain constant kinetic temperature during equilibration by scaling the velocities by (desired temperature/current kinetic temperature)$^{1/2}$, say at every MD step. However, because temperature is not a fixed parameter in constant energy MD simulations, the state point reached at the end of equilibration is typically only close to the desired one, often frustrating reproduction of independently obtained results, for comparison purposes. As a more effective alternative to the crude velocity scaling technique, either TA1 or TA2 can be used to fix the kinetic temperature during equilibration, with the tolerance $\tau$ adjusted for approaching a particular state point as closely as desired at the end of equilibration, as illustrated in Figs. 1 and 2 for the TA1 and TA2, respectively. For the TA1, the average number of iterations per MD step over the equilibra-

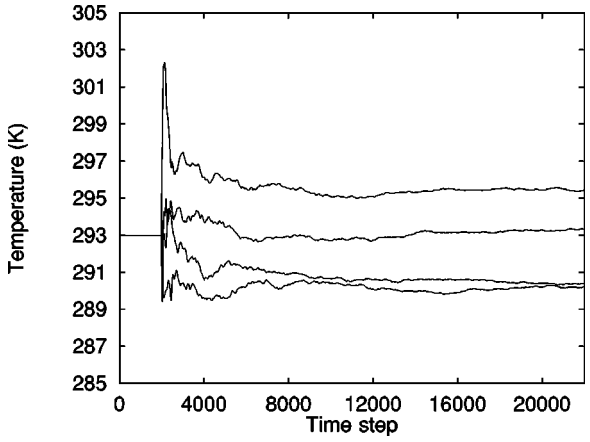


FIG. 1. Thermodynamic temperature vs time step in constant energy MD simulations of 500 Lennard-Jones rigid molecules ($CH_2Cl_2$), with 2000 equilibration steps and 20 000 production steps. The desired temperature is 293 K. At the end of equilibration the temperature accumulator is reset to zero. The bottom curve is obtained with velocity scaling at every step during the equilibration phase. The other curves are obtained using TA1 during equilibration. Starting with the lowest curve and counting up, the tolerance values used are $\tau=0.1$, 0.7, and 0.8, respectively. Of these values, the optimal one for attaining the desired set point temperature, using TA1, is in this case $\tau=0.7$.

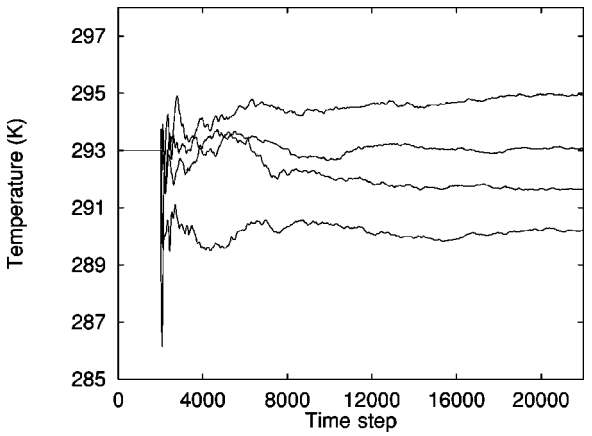


FIG. 2. Thermodynamic temperature vs time step in constant energy MD simulations of 500 Lennard-Jones rigid molecules ($CH_2Cl_2$), with 2000 equilibration steps and 20 000 production steps. The desired temperature is 293 K. At the end of equilibration the temperature accumulator is reset to zero. The bottom curve is obtained with velocity scaling at every step during the equilibration phase. The other curves are obtained using TA2 during equilibration. Starting with the lowest curve and counting up, the tolerance values used are $\tau=0.1$, 0.2, and 0.3, respectively. Of these values, the optimal one for attaining the desired set point temperature, using TA2, is in this case $\tau=0.2$.

tion period was 0.13, 0.013, and 0.0065 for $\tau=0.1$, 0.7, and 0.8, respectively. For the TA2, the average number of iterations per MD step over the equilibration period was 61.5, 43.1, and 33.8 for $\tau=0.1$, 0.2, and 0.3, respectively. The reason for the large difference between the convergence rates of TA1 and TA2 is explained shortly.

The BTA attempts to maintain a given temperature constant. As noted before, this temperature will drift however because of numerical integration error. The correction technique in TA1 ensures that the temperature remains at the desired value at every step of the simulation. Because the correction technique is a linearized expansion-based scheme, it requires relatively small corrections to converge. Hence in the first step only of equilibration with TA1, the kinetic temperature is brought to, or near, the desired value using velocity scaling. The remainder of the equilibration is performed solely with TA1. Similarly, the TA2 is a linearized expansion-based algorithm, hence it requires small corrections to converge. Therefore in the first step only of equilibration with TA2, the kinetic temperature is also brought to, or near, the desired value using velocity scaling, and the remainder of the equilibration is performed solely with TA2.

Second, we perform constant kinetic temperature simulations with the BTA, TA1, and TA2, and compare constraint conservation results. Figure 3 compares kinetic temperatures in constant kinetic temperature simulations using TA1, TA2, and BTA. A tolerance $\tau=0.01$ was used for both TA1 and TA2. In the simulations with TA1 and TA2, the kinetic temperature was fixed during equilibration using also TA1 and TA2, respectively, as described above, whereas velocity scaling was used for this purpose in the simulation with BTA. For the above value of the tolerance, the average number of iterations per MD step over the entire production period was 3 for TA1 and 174 for TA2. Figures 4 and 5 show comparisons on an expanded scale between the kinetic temperature

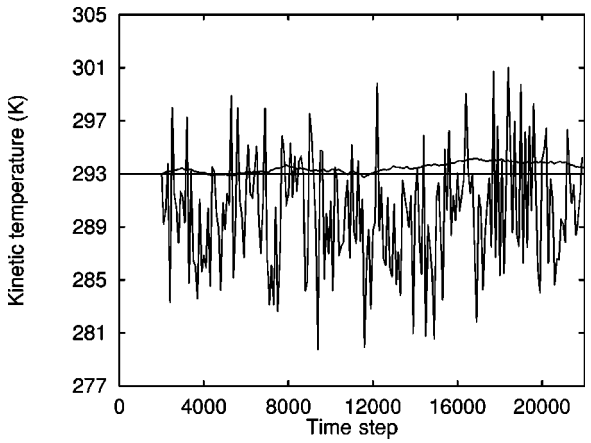


FIG. 3. Kinetic temperature vs time step for four MD simulations of 500 Lennard-Jones rigid molecules ($CH_2Cl_2$), with 2000 equilibration steps and 20 000 production steps in each. The two overlapping horizontal lines are from constant kinetic temperature MD simulations using TA1 and TA2, respectively, for the entire simulation runs, with desired kinetic temperature of 293 K and tolerance value $\tau=0.01$ for both simulations. The drifting curve in the neighborhood of the horizontal line is from a constant kinetic temperature MD simulation using the BTA during production and velocity scaling at every step during equilibration, with desired kinetic temperature of 293 K also. The background curve is from a constant energy MD simulation with desired (thermodynamic) temperature of 293 K, where the kinetic temperature is shown every 100 steps only to prevent cluttering. Velocity scaling is also used at every step to fix the kinetic temperature during equilibration of this simulation.

from the simulation with BTA and the kinetic temperatures from the simulations with TA1 and TA2, respectively.

Figures 3, 4, and 5 show clearly that the BTA by itself suffers from numerical drift in the constant kinetic temperature constraint, hence the need for the two more accurate

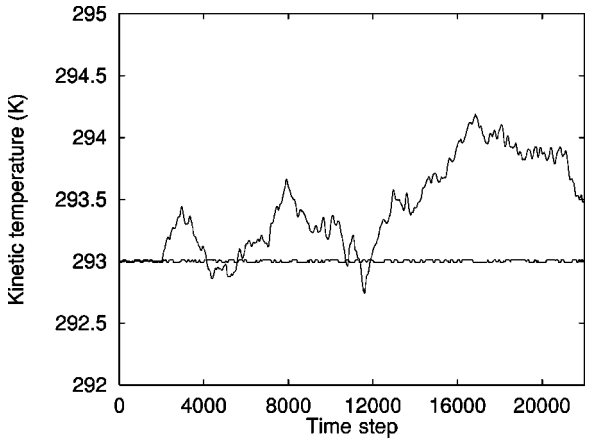


FIG. 4. Kinetic temperature vs time step for two constant kinetic temperature MD simulations of 500 Lennard-Jones rigid molecules ($CH_2Cl_2$), with 2000 equilibration steps and 20 000 production steps, and desired kinetic temperature of 293 K. The horizontal line is from a constant kinetic temperature MD simulation using TA1 for the entire simulation run with tolerance value $\tau=0.01$. The drifting curve is from a constant kinetic temperature MD simulation using the BTA during production and velocity scaling at every step during equilibration.

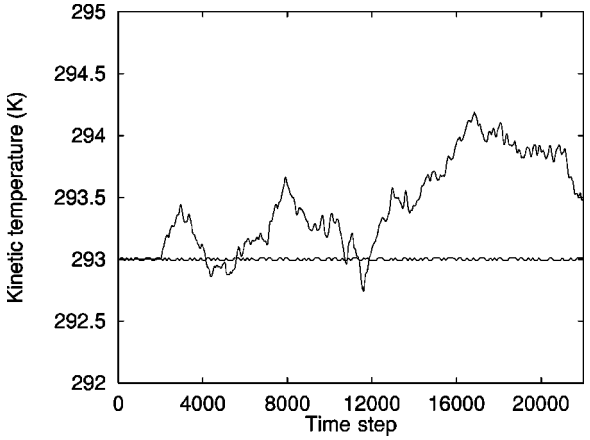


FIG. 5. Kinetic temperature vs time step for two constant kinetic temperature MD simulations of 500 Lennard-Jones rigid molecules ($CH_2Cl_2$), with 2000 equilibration steps and 20 000 production steps, and desired kinetic temperature of 293 K. The horizontal line is from a constant kinetic temperature MD simulation using TA2 for the entire simulation run with tolerance value $\tau = 0.01$, where the kinetic temperature is shown every 100 steps only to prevent cluttering. The drifting curve is from a constant kinetic temperature MD simulation using the BTA during production and velocity scaling at every step during equilibration.

thermostat algorithms, TA1 and TA2. From the above results it is clear that TA1 requires in general fewer iterations to converge within a desired tolerance $\tau$ than does TA2. This faster convergence of the TA1 can be attributed to the fact that the iterative correction in the TA1 is performed on the already constrained motion (i.e., through the BTA), while the iterative correction in the TA2 is performed on unconstrained motion, as described in Secs. III and IV, respectively. On the other hand, TA2 is easier to implement than TA1 for that same reason. Figure 6 shows the ratios of the translational to rotational kinetic energies for the two simulations using TA1 and TA2, respectively. The average ratio over the entire production period was 0.99 for both simulations.

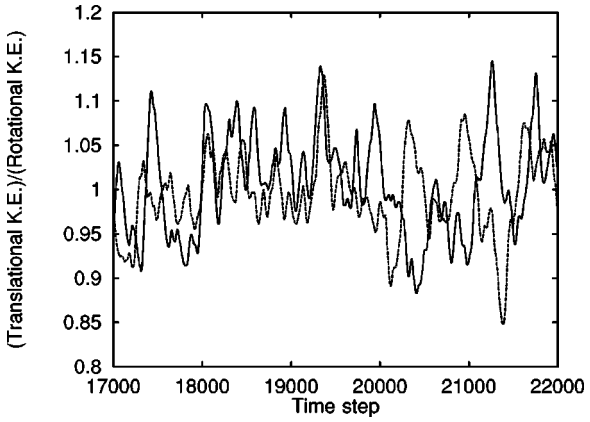


FIG. 6. Ratio of translational to rotational kinetic energies for the constant kinetic temperature simulations performed with the TA1 (solid line) and TA2 (dashed line). Ratios are shown only for the last 5000 steps of the simulations to avoid cluttering.

## VI. CONCLUSION

In this article, generalized equations were derived for the motion of a rigid body under general nonholonomic constraints. These equations were used to develop two molecular thermostat algorithms TA1 and TA2, for constant kinetic temperature MD simulations of rigid molecules. Results from MD simulations of a system of methylene chloride rigid molecules exhibited the good performance of both TA1 and TA2 and their relative advantages. The molecular algorithms presented here complement atomistic constraint algorithms described previously [4,5]. In the context of these atomistic methods, the TA1 is the molecular approach counterpart of the direct method [4,5], albeit with a drift correction scheme, and the TA2 is the analog of the GSHAKE [4,5] algorithm. Finally, a generalized Gauss principle of least constraint was derived to provide a formal link between these atomistic and molecular approaches.

## ACKNOWLEDGMENTS

This research was partly funded by the United Kingdom EPSRC under Grant No. GR/L49956 and by Unilever Research. The authors would like to thank Manchester Computing for use of the SGI Origin 2000 through the EPSRC funded Class 3 service.

## APPENDIX A: ERROR ANALYSIS FOR TA1

Any technique designed to eliminate or reduce within a desired tolerance the numerical constraint drift must not introduce consequently additional numerical errors (i.e., of lower order in the time-step) to those in the integration algorithm and the original method (e.g., the BTA). We provide here an error analysis for the TA1, which shows that it does not introduce errors into the center of mass velocities additional to those present in the BTA.

The center of mass velocities generated by the BTA can be represented by the Taylor expansion Eq. (22). The last term in Eq. (22) contains $\lambda(t_0)$ and the highest power $\delta t$. Assuming the integration algorithm has an error in the center of mass velocities of $O(\delta t^{m+1})$, the equivalence of the Taylor expansion and the integration algorithm implies that the highest term in the Taylor expansion is of $O(\delta t^m)$, hence $\delta t \lambda(t_0)$ is of $O(\delta t^m)$. Therefore $\lambda(t_0)$ is of $O(\delta t^{m-1})$, or

$$\lambda(t_0) = \beta + O(\delta t^m), \tag{A1}$$

where $\beta$ is some estimated or approximated value of $\lambda(t_0)$. Comparison of Eq. (22) with Eq. (23) shows that the drift correction technique involves the approximation of $\lambda(t_0)$ by $[\lambda(t_0)+\gamma]$ in Eq. (23). Accordingly, replacing $\beta$ by $[\lambda(t_0)+\gamma]$, Eq. (A1) becomes

$$[\lambda(t_0)+\gamma] = \lambda(t_0) + O(\delta t^m). \tag{A2}$$

Inserting Eq. (A2) back into Eq. (23), the final constrained center of mass velocities given by the correction technique can be written as

$$\dot{\mathbf{r}}_i(t_0+\delta t,\gamma)=\dot{\mathbf{r}}_i(t_0)+\frac{\delta t}{M_i}\mathbf{F}_i(t_0)-\delta t\lambda(t_0)\dot{\mathbf{r}}_i(t_0)+O(\delta t^{m+1}) \quad (i=1,\ldots,N). \tag{A3}$$

By comparing Eq. (A3) with Eq. (22), we can write

$$\dot{\mathbf{r}}_i[\mathrm{TA1}]=\dot{\mathbf{r}}_i[\mathrm{BTA}]+O(\delta t^{m+1}) \quad (i=1,\ldots,N). \tag{A4}$$

On the other hand, from the assumed $O(\delta t^{m+1})$ of error in the center of mass velocities in the BTA, we can write

$$\dot{\mathbf{r}}_i[\mathrm{BTA}]=\dot{\mathbf{r}}_i[\mathrm{exact}](t_0+\delta t)+O(\delta t^{m+1}), \tag{A5}$$

where $\dot{\mathbf{r}}_i[\mathrm{exact}]$ is the trajectory obtained ideally from an exact analytical solution of the equations of motion. Finally, inserting Eq. (A5) into Eq. (A4) gives

$$\dot{\mathbf{r}}_i[\mathrm{TA1}]=\dot{\mathbf{r}}_i[\mathrm{exact}](t_0+\delta t)+O(\delta t^{m+1}). \tag{A6}$$

Equation (A4) shows that the correction technique, or TA1, introduces no additional errors into the center of mass velocities of the BTA. Equivalently, comparison of Eq. (A6) with Eq. (A5) shows that the velocity trajectories from the BTA and the TA1 are numerically equivalent, where in the TA1, however, the constant kinetic temperature constraint is satisfied at every MD time step.

## APPENDIX B: ERROR ANALYSIS FOR TA2

We provide here an error analysis for the TA2, which shows that it does not introduce errors into the center of mass velocities or angular velocities additional to those present in the BTA. The center of mass velocities and angular velocities generated by the BTA can be represented by the Taylor expansions Eqs. (29) and (30), respectively. The last term in each of these equations contains $\lambda(t_0)$ and the highest power $\delta t$. Assuming the integration algorithm has an error in the center of mass velocities of $O(\delta t^{m+1})$ and an error in the angular velocities of $O(\delta t^{m'+1})$, the equivalence of the Taylor expansions and the integration algorithm implies that the highest term in the Taylor expansions is of $O(\delta t^{m})$ and $O(\delta t^{m'})$, respectively. Hence, in Eq. (29), $\delta t\lambda(t_0)$ is of $O(\delta t^{m})$ and therefore $\lambda(t_0)$ is of $O(\delta t^{m-1})$, or

$$\lambda(t_0)=\beta+O(\delta t^{m}) \tag{B1}$$

and, in Eq. (30), $\delta t\lambda(t_0)$ is of $O(\delta t^{m'})$ and therefore $\lambda(t_0)$ is of $O(\delta t^{m'-1})$, or

$$\lambda(t_0)=\beta+O(\delta t^{m'}), \tag{B2}$$

where $\beta$ is some estimated or approximated value of $\lambda(t_0)$. In TA2, $\lambda(t_0)$ is replaced by $\eta$, as described in Sec. IV. Accordingly, replacing $\beta$ by $\eta$, Eq. (B1) becomes

$$\eta=\lambda(t_0)+O(\delta t^{m}) \tag{B3}$$

and Eq. (B2) leads to

$$\eta=\lambda(t_0)+O(\delta t^{m'}). \tag{B4}$$

Inserting Eq. (B3) back into Eq. (31), the constrained center of mass velocities given by TA2 can be written as

$$\dot{\mathbf{r}}_i(t_0+\delta t)=\dot{\mathbf{r}}'_i(t_0+\delta t)-\delta t\lambda(t_0)\dot{\mathbf{r}}_i(t_0)+O(\delta t^{m+1}) \quad (i=1,\ldots,N). \tag{B5}$$

Inserting Eq. (B4) back into Eq. (32), the constrained angular velocities given by TA2 can be written as

$$\omega_i^j(t_0+\delta t)=\omega_i'^j(t_0+\delta t)-\delta t\lambda(t_0)\omega_i^j(t_0)+O(\delta t^{m'+1}) \quad (i=1,\ldots,3;\ \ j=1,\ldots,N). \tag{B6}$$

Comparing Eqs. (B5) and (B6) with Eqs. (29) and (30), respectively, we can write

$$\dot{\mathbf{r}}_i[\mathrm{TA2}]=\dot{\mathbf{r}}_i[\mathrm{BTA}]+O(\delta t^{m+1}) \quad (i=1,\ldots,N),$$

$$\omega_i^j[\mathrm{TA2}]=\omega_i^j[\mathrm{BTA}]+O(\delta t^{m'+1}) \quad (i=1,\ldots,3;\ \ j=1,\ldots,N). \tag{B7}$$

On the other hand, from the assumed $O(\delta t^{m+1})$ and $O(\delta t^{m'+1})$ of errors in the center of mass velocities and angular velocities in the BTA, respectively, we can write

$$\dot{\mathbf{r}}_i[\mathrm{BTA}]=\dot{\mathbf{r}}_i[\mathrm{exact}]+O(\delta t^{m+1}) \quad (i=1,\ldots,N),$$

$$\omega_i^j[\mathrm{BTA}]=\omega_i^j[\mathrm{exact}]+O(\delta t^{m'+1}) \quad (i=1,\ldots,3;\quad j=1,\ldots,N), \tag{B8}$$

where $\dot{\mathbf{r}}_i[\mathrm{exact}]$ and $\omega_i^j[\mathrm{exact}]$ are the velocities obtained ideally from an exact analytical solution of the constrained equations of motion. Finally, inserting Eq. (B8) into Eq. (B7) gives

$$\dot{\mathbf{r}}_i[\mathrm{TA2}]=\dot{\mathbf{r}}_i[\mathrm{exact}]+O(\delta t^{m+1}) \quad (i=1,\ldots,N),$$

$$\omega_i^j[\mathrm{TA2}]=\omega_i^j[\mathrm{exact}]+O(\delta t^{m'+1}) \quad (i=1,\ldots,3;\ \ j=1,\ldots,N). \tag{B9}$$

Comparison of Eq. (B9) with Eq. (B8) shows that the velocity trajectories from the BTA and from the TA2 are numerically equivalent, where in the TA2, however, the constant kinetic temperature constraint is satisfied at every MD time step.

## APPENDIX C: GENERALIZED GAUSS PRINCIPLE

As mentioned before, the atomistic approach for applying nonholonomic constraints in MD simulations exploited initially Gauss's principle of least constraint. To establish a common theoretical framework for the molecular approach constraint algorithms, such as the BTA, TA1, and TA2 introduced in this work, and the atomistic approach algorithms [4,5], such as GSHAKE and the direct method, we derive here a generalized form of Gauss's principle, and then show that it leads to the same equations of motion, Eq. (2), used to formulate the present molecular approach.

For a system of $N$ particles with masses $m_i$, Gauss's prin-

ciple of least constraint [17,18,24,25]

$$\delta\left[\sum_{i=1}^{N}\frac{m_i^{-1}}{2}(\mathbf{F}_i-m_i\ddot{\mathbf{r}}_i)^2\right]=0,\quad \delta\mathbf{r},\delta\dot{\mathbf{r}}=0 \tag{C1}$$

states that at any point along the actual path of the motion in $(\mathbf{r},\dot{\mathbf{r}},\ddot{\mathbf{r}})$ space, the bracketed quantity is minimum with respect to variations in the accelerations satisfying any constraints present, keeping the coordinates and velocities fixed. The system of $N$ particles is assumed to be subject in general to both holonomic and nonholonomic constraints. Alternatively, Eq. (C1) can be written in terms of the constraint forces

$$\delta\left[\sum_{i=1}^{N}\frac{m_i^{-1}}{2}(\mathbf{F}_i^c)^2\right]=0,\quad \delta\mathbf{r},\delta\dot{\mathbf{r}}=\mathbf{0}. \tag{C2}$$

Carrying out the variation, the left side of Eq. (C1) gives

$$\delta\left[\sum_{i=1}^{N}\frac{1}{2m_i}(\mathbf{F}_i-m_i\ddot{\mathbf{r}}_i)^2\right]=\sum_{i=1}^{N}\frac{1}{m_i}(\mathbf{F}_i-m_i\ddot{\mathbf{r}}_i)\cdot\delta(\mathbf{F}_i-m_i\ddot{\mathbf{r}}_i)$$

$$=-\sum_{i=1}^{N}(\mathbf{F}_i-m_i\ddot{\mathbf{r}}_i)\cdot\delta\ddot{\mathbf{r}}_i,$$

$$\delta\mathbf{r},\delta\dot{\mathbf{r}}=\mathbf{0}, \tag{C3}$$

where the last equality follows from the vanishing of the variation of the applied forces $\mathbf{F}_i(\mathbf{r},\dot{\mathbf{r}},t)$, at fixed coordinates and velocities

$$\delta\mathbf{F}_i=\sum_{j=1}^{N}\delta\mathbf{r}_j\cdot\frac{\partial\mathbf{F}_i}{\partial\mathbf{r}_j}+\sum_{j=1}^{N}\delta\dot{\mathbf{r}}_j\cdot\frac{\partial\mathbf{F}_i}{\partial\dot{\mathbf{r}}_j}=0,\quad \delta\mathbf{r},\delta\dot{\mathbf{r}}=\mathbf{0}. \tag{C4}$$

Using Eq. (C3), Gauss's principle, Eq. (C1), assumes the equivalent form

$$\sum_{i=1}^{N}(\mathbf{F}_i-m_i\ddot{\mathbf{r}}_i)\cdot\delta\ddot{\mathbf{r}}_i=0,\quad \delta\mathbf{r},\delta\dot{\mathbf{r}}=\mathbf{0}. \tag{C5}$$

We wish first to recast Eq. (C5) in terms of generalized coordinates. To this end, we effect a point transformation to a set of $\gamma$ generalized coordinates $q$

$$\mathbf{r}_i=\mathbf{r}_i(q_1,\ldots,q_\gamma,t),\quad i=1,\ldots,N. \tag{C6}$$

In general $\gamma\leqslant 3N$. For example, if no holonomic constraints are incorporated implicitly in the point transformation, Eq. (C6), then $\gamma=3N$. On the other hand, in the case of a rigid body $\gamma=6$. From Eq. (C6) it follows that

$$\delta\mathbf{r}_i=\sum_{j=1}^{\gamma}\frac{\partial\mathbf{r}_i}{\partial q_j}\delta q_j;\quad i=1,\ldots,N. \tag{C7}$$

Differentiating Eq. (C7) twice with respect to time and evaluating the variation at fixed coordinates and velocities, gives

$$\delta\ddot{\mathbf{r}}_i=\sum_{j=1}^{\gamma}\frac{\partial\mathbf{r}_i}{\partial q_j}\delta\ddot{q}_j,\quad \delta q,\delta\dot{q}=0. \tag{C8}$$

Inserting Eq. (C8) into Eq. (C5) yields

$$\sum_{j=1}^{\gamma}\left[\sum_{i=1}^{N}\left(\mathbf{F}_i\cdot\frac{\partial\mathbf{r}_i}{\partial q_j}-m_i\ddot{\mathbf{r}}_i\cdot\frac{\partial\mathbf{r}_i}{\partial q_j}\right)\right]\delta\ddot{q}_j=0,\quad \delta q,\delta\dot{q}=0. \tag{C9}$$

The common quantity in brackets is easily recast [20] in generalized coordinates and Eq. (C9) then becomes

$$\sum_{j=1}^{\gamma}\left[\frac{d}{dt}\left(\frac{\partial T}{\partial\dot{q}_j}\right)-\frac{\partial T}{\partial q_j}-Q_j\right]\delta\ddot{q}_j=0,\quad \delta q,\delta\dot{q}=0, \tag{C10}$$

where the $Q_j$ are the generalized applied forces and $T$ is the kinetic energy. Equation (C10) is the desired generalized coordinates form of Eq. (C5). We now recast Eq. (C10) in the form of a minimum principle. For the kinetic energy $T(q,\dot{q},t)$ we can write

$$\frac{d}{dt}\left(\frac{\partial T}{\partial\dot{q}_j}\right)=\sum_{i=1}^{\gamma}\frac{\partial}{\partial q_i}\left(\frac{\partial T}{\partial\dot{q}_j}\right)\dot{q}_i+\sum_{i=1}^{\gamma}\frac{\partial}{\partial\dot{q}_i}\left(\frac{\partial T}{\partial\dot{q}_j}\right)\ddot{q}_i+\frac{\partial}{\partial t}\left(\frac{\partial T}{\partial\dot{q}_j}\right). \tag{C11}$$

Evaluating the variation of Eq. (C11) at fixed coordinates and velocities gives

$$\delta\left[\frac{d}{dt}\left(\frac{\partial T}{\partial\dot{q}_j}\right)\right]=\sum_{i=1}^{\gamma}\left(\frac{\partial^2 T}{\partial\dot{q}_j\partial\dot{q}_i}\right)\delta\ddot{q}_i$$

$$=\sum_{i=1}^{\gamma}M_{ij}(q,t)\,\delta\ddot{q}_i,\quad \delta q,\delta\dot{q}=0, \tag{C12}$$

where $M_{ij}$ is evidently a symmetric matrix. Solving for $\delta\ddot{q}_i$ yields

$$\delta\ddot{q}_i=\sum_{j=1}^{\gamma}M_{ij}^{-1}\delta\left[\frac{d}{dt}\left(\frac{\partial T}{\partial\dot{q}_j}\right)\right],\quad \delta q,\delta\dot{q}=0. \tag{C13}$$

By means of Eq. (C13), the left side of Eq. (C10) can be written as

$$\sum_{i=1}^{\gamma}\left[\frac{d}{dt}\left(\frac{\partial T}{\partial\dot{q}_i}\right)-\frac{\partial T}{\partial q_i}-Q_i\right]\delta\ddot{q}_i=\sum_{i=1}^{\gamma}\left[\frac{d}{dt}\left(\frac{\partial T}{\partial\dot{q}_i}\right)-\frac{\partial T}{\partial q_i}-Q_i\right]$$

$$\times\left\{\sum_{j=1}^{\gamma}M_{ij}^{-1}\delta\left[\frac{d}{dt}\left(\frac{\partial T}{\partial\dot{q}_j}\right)\right]\right\},$$

$$\delta q,\delta\dot{q}=0. \tag{C14}$$

However,

$$\delta\left[\frac{d}{dt}\left(\frac{\partial T}{\partial\dot{q}_j}\right)\right]=\delta\left[\frac{d}{dt}\left(\frac{\partial T}{\partial\dot{q}_j}\right)-\frac{\partial T}{\partial q_j}-Q_j\right],\quad \delta q,\delta\dot{q}=0, \tag{C15}$$

because the variations of $\partial T/\partial q_j$ and $Q_j(q,\dot{q},t)$ both vanish at fixed coordinates and velocities. Inserting Eq. (C15) into Eq. (C14) gives

$$\begin{aligned}
&\sum_{i=1}^{\gamma}\left[\frac{d}{dt}\left(\frac{\partial T}{\partial \dot{q}_i}\right)-\frac{\partial T}{\partial q_i}-Q_i\right]\delta\ddot{q}_i \\
&\quad=\sum_{i,j=1}^{\gamma} M_{ij}^{-1}\left[\frac{d}{dt}\left(\frac{\partial T}{\partial \dot{q}_i}\right)-\frac{\partial T}{\partial q_i}-Q_i\right] \\
&\qquad\times\delta\left[\frac{d}{dt}\left(\frac{\partial T}{\partial \dot{q}_j}\right)-\frac{\partial T}{\partial q_j}-Q_j\right] \\
&\quad=\sum_{i,j=1}^{\gamma}\frac{M_{ij}^{-1}}{2}\delta\left\{\left[\frac{d}{dt}\left(\frac{\partial T}{\partial \dot{q}_i}\right)-\frac{\partial T}{\partial q_i}-Q_i\right]\right. \\
&\qquad\left.\times\left[\frac{d}{dt}\left(\frac{\partial T}{\partial \dot{q}_j}\right)-\frac{\partial T}{\partial q_j}-Q_j\right]\right\} \\
&\quad=\delta\left\{\sum_{i,j=1}^{\gamma}\frac{M_{ij}^{-1}}{2}\left[\frac{d}{dt}\left(\frac{\partial T}{\partial \dot{q}_i}\right)-\frac{\partial T}{\partial q_i}-Q_i\right]\right. \\
&\qquad\left.\times\left[\frac{d}{dt}\left(\frac{\partial T}{\partial \dot{q}_j}\right)-\frac{\partial T}{\partial q_j}-Q_j\right]\right\},\quad \delta q,\delta\dot{q}=0,
\end{aligned} \tag{C16}$$

where use was made of the symmetry of $M_{ij}^{-1}(q,t)$ in the second equality, and of its vanishing variation at fixed coordinates and velocities in the last equality. Finally, combining Eq. (C16) with Eq. (C10) leads to

$$\begin{aligned}
&\delta\left\{\sum_{i,j=1}^{\gamma}\frac{M_{ij}^{-1}}{2}\left[\frac{d}{dt}\left(\frac{\partial T}{\partial \dot{q}_i}\right)-\frac{\partial T}{\partial q_i}-Q_i\right]\right. \\
&\qquad\left.\times\left[\frac{d}{dt}\left(\frac{\partial T}{\partial \dot{q}_j}\right)-\frac{\partial T}{\partial q_j}-Q_j\right]\right\}=0,\quad \delta q,\delta\dot{q}=0
\end{aligned} \tag{C17}$$

which states that at any point along the actual path of the motion in $(q,\dot{q},\ddot{q})$-space, the quantity in curly brackets minimum with respect to variations in the generalized accelerations satisfying any constraints present, keeping the generalized coordinates and velocities fixed. Eq. (C17) is a generalized form of Gauss's principle of least constraint. Recognizing that the quantities in brackets are equal to the generalized constraint forces, Eq. (C17) can also be written in the alternative compact form

$$\delta\left[\sum_{i,j=1}^{\gamma}\frac{M_{ij}^{-1}}{2}Q_i^cQ_j^c\right]=0,\quad \delta q,\delta\dot{q}=0. \tag{C18}$$

In the case of Cartesian coordinates we have $M_{ij}=m_i\delta_{ij}$, and Eqs. (C17) and (C18) reduce to the forms of Eqs. (C1) and (C2), respectively.

We now consider the rigid body of Sec. II and show that the same equations of motion, Eq. (2), follow from an application of the generalized Gauss principle, Eq. (C17). Carrying out the variation in Eq. (C17) (with $\gamma=6$) and retracing the steps above leads back to Eq. (C10). Differentiating Eq. (1) with respect to time gives

$$\frac{d\sigma_l}{dt}=\sum_{j=1}^{6}\frac{\partial\sigma_l}{\partial q_j}\dot{q}_j+\sum_{j=1}^{6}\frac{\partial\sigma_l}{\partial\dot{q}_j}\ddot{q}_j+\frac{\partial\sigma_l}{\partial t}=0,\quad l=1,\ldots,n \tag{C19}$$

the variation of which at fixed coordinates and velocities leads to

$$\delta\left(\frac{d\sigma_l}{dt}\right)=\sum_{j=1}^{6}\frac{\partial\sigma_l}{\partial\dot{q}_j}\delta\ddot{q}_j=0,\quad \delta q,\delta\dot{q}=0,\quad l=1,\ldots,n. \tag{C20}$$

From the statement of the generalized Gauss principle, Eqs. (C10) and (C20) hold simultaneously. Accordingly, multiplying each of the $n$ constraints in Eq. (C20) by a corresponding Lagrange multiplier, summing over the constraints, and adding the resulting sum to Eq. (C10), gives

$$\begin{aligned}
&\sum_{j=1}^{6}\left[\frac{d}{dt}\left(\frac{\partial T}{\partial\dot{q}_j}\right)-\frac{\partial T}{\partial q_j}-Q_j+\sum_{l=1}^{n}\lambda_l\frac{\partial\sigma_l}{\partial\dot{q}_j}\right]\delta\ddot{q}_j=0, \\
&\qquad\delta q,\delta\dot{q}=0.
\end{aligned} \tag{C21}$$

Following the usual arguments [20,24] of the Lagrange multiplier technique, the terms in brackets in Eq. (C21) all vanish, leading to the equations of motion, Eq. (2).


[1] A. T. Allen and D. J. Tildesley, *Computer Simulation of Liquids* (Oxford University Press, Oxford, 1992).

[2] Wm. G. Hoover, *Computational Statistical Mechanics*, Vol. 11 of *Studies in Modern Thermodynamics* (Elsevier, Amsterdam, 1991).

[3] D. C. Rapaport, *The Art Of Molecular Dynamics Simulation* (Cambridge University Press, Cambridge, 1995).

[4] R. Kutteh, J. Chem. Phys. **111**, 1394 (1999).

[5] R. Kutteh, Comput. Phys. Commun. **119**, 159 (1999).

[6] J. P. Ryckaert, G. Ciccotti, and H. J. C. Berendsen, J. Comput. Phys. **23**, 327 (1977).

[7] J. P. Ryckaert, Mol. Phys. **55**, 549 (1985).

[8] G. Ciccotti and J. P. Ryckaert, Comput. Phys. Rep. **4**, 345 (1986).

[9] R. Kutteh and T. P. Straatsma, in *Reviews in Computational Chemistry*, edited by K. B. Lipkowitz and D. B. Boyd (Wiley, New York, 1998), Vol. 12, pp. 75–136.

[10] A. Kol, B. B. Laird, and B. J. Leimkuhler, J. Chem. Phys. **107**, 2580 (1997).

[11] I. P. Omelyan, Phys. Rev. E **58**, 1169 (1998).

[12] I. P. Omelyan, Comput. Phys. Commun. **109**, 171 (1998).

[13] I. P. Omelyan, Comput. Phys. **12**, 97 (1998).

[14] A. Dullweber, B. Leimkuhler, and R. McLachlan, J. Chem. Phys. **107**, 5840 (1997).

[15] G. R. Kneller and K. Hinsen, Phys. Rev. E **50**, 1559 (1994).
[16] W. Smith and T. R. Forester, J. Comput. Chem. **19**, 102 (1998).
[17] J. I. Neimark and N. A. Fufaev, *Dynamics of Nonholonomic Systems* (American Mathematical Society, Providence, RI, 1972), Vol. 33.
[18] L. A. Pars, *A Treatise On Analytical Dynamics* (Heinemann, London, 1965).
[19] D. Frenkel and B. Smit, *Understanding Molecular Simulation* (Academic, New York, 1996).
[20] H. Goldstein, *Classical Mechanics*, 2nd ed. (Addison-Wesley, New York, 1981).
[21] H. Rund, *The Hamilton-Jacobi Theory In The Calculus Of Variations* (Krieger, New York, 1973).
[22] E. J. Saletan and A. H. Cromer, *Theoretical Mechanics* (Wiley, New York, 1971).
[23] J. R. Ray, Am. J. Phys. **40**, 179 (1972).
[24] C. Lanczos, *The Variational Principles of Mechanics*, 4th ed. (Dover, New York, 1986).
[25] E. T. Whittaker, *A Treatise On The Analytical Dynamics Of Particles And Rigid Bodies*, 4th ed. (Dover, New York, 1937).
[26] S. W. McCuskey, *An Introduction To Advanced Dynamics* (Addison-Wesley, New York, 1959).
[27] M. Ferrario and M. W. Evans, Chem. Phys. **72**, 141 (1982).